

TESTING RADIATIVELY-INEFFICIENT ACCRETION FLOW THEORY: AN *XMM-NEWTON* OBSERVATION OF NGC 3998

A. PTAK

The Johns Hopkins University, Department of Physics and Astronomy, Baltimore, MD 21218

Y. TERASHIMA

Institute of Space and Astronautical Science, 3-1-1 Yoshinodai, Sagamihara, Kanagawa 229-8510, Japan

L. C. HO

The Observatories of the Carnegie Institution of Washington, 813 Santa Barbara S., Pasadena, CA 91101-1292

E. QUATAERT

University of California at Berkeley, Astronomy Department, Berkeley, CA 94720

Accepted for publication in ApJ

ABSTRACT

We present the results of a 10 ks *XMM-Newton* observation of NGC 3998, a “type-I” LINER galaxy (i.e., with significant broad H α emission). Our goal is to test the extent to which radiatively-inefficient accretion flow (RIAF) models and/or scaled-down AGN models are consistent with the observed properties of NGC 3998. A power-law fit to the *XMM-Newton* spectra results in a power-law slope of $\Gamma = 1.9$ and 2-10 keV flux of 1.1×10^{-11} erg cm $^{-2}$ s $^{-1}$, in excellent agreement with previous hard X-ray observations. The OM UV flux at 2120Å appears to be marginally resolved, with $\sim 50\%$ of the flux extended beyond 2”. The nuclear component of the 2120Å flux is consistent with an extrapolation of the X-ray power-law, although $\sim 50\%$ of the flux may be absorbed. The OM U flux lies significantly above the X-ray power-law extrapolation and contains a significant contribution from extragalactic emission. The upper-limit for narrow Fe-K emission derived from the *XMM-Newton* spectra is 33 eV (for $\Delta\chi^2 = 2.7$). The upper-limit for narrow Fe-K emission derived from a combined fit of the *XMM-Newton* and *BeppoSAX* spectra is 25 eV, which is one of the strictest limits to date for any AGN. This significantly rules out Fe-K emission as is expected to be observed in typical Seyfert 1 galaxies. The X-ray flux of NGC 3998 has not been observed to vary significantly (at $> 30\%$ level) within the X-ray observations, and only between observations at a level of $\sim 50\%$, which is also in contrast to typical Seyfert 1 galaxies. The lack of *any* reflection features suggests that any optically-thick, geometrically-thin accretion disk must be truncated, probably at a radius of order 100-300 (in Schwarzschild units). RIAF models fit the UV to X-ray spectral energy distribution of NGC 3998 reasonably well. In these models the mid-IR flux also constrains the emission from any outer thin disk component that might be present. The UV to X-ray SED is also consistent with a Comptonized thin disk with a very low accretion rate ($\dot{M} < 10^{-5} \dot{M}_{\text{Edd}}$), in which case the lack of Fe-K emission may be due to an ionized accretion disk. Accretion models in general do not account for the observed radio flux of NGC 3998, and the radio flux may be due to a jet. Recent jet models may also be consistent with the nuclear fluxes of NGC 3998 in general, including the X-ray, optical/UV and mid-IR bands. The (ground-based) near-IR to optical photometric data for the nuclear region of NGC 3998 contains large contributions from extra-nuclear emission. We also derive nuclear fluxes using archival HST WFPC2 data, resulting in meaningful constraints to the nuclear SED of NGC 3998 in the optical band. We discuss a possible OM U band and USNO-B detection of the NGC 3998 ULX.

Subject headings: X-rays: galaxies — galaxies: individual (NGC 3998) — accretion, accretion disks

1. INTRODUCTION

Since LINERs (low-ionization nuclear emission-line regions; Heckman 1980) were first identified as a class the nature of the source of ionization has been debated, with the two main possibilities being a starburst or AGN nuclear source. If an AGN is responsible for the ionization, the next question is how similar are these AGN to Seyferts and QSOs. An interesting development has been the discovery of broad H α emission in many LINERs (Ho, Filippenko, & Sargent 1997). These LINERs are almost certainly AGN powered, particularly when

they are observed in early-type galaxies where outflows from massive stars and/or supernovae are not expected to be relevant. Early-type galaxies also tend to harbor very massive central black holes, making broad-line LINERs observed in early-type galaxies ideal laboratories for studying (potentially) low accretion rate physics. Of course, this is assuming that the X-ray emission is isotropic and scales with accretion rate, however alternatively the accretion energy may be dissipated anisotropic and/or non-radiatively (i.e., in outflows; Di Matteo et al. 2000).

NGC 3998 is an SO galaxy at a distance of 14.1 Mpc (Tonry et al. 2001). Its H α line contains a broad component with 37% of the H α + [N II] flux and a FWHM of ~ 2000 km s $^{-1}$ (Ho, Filippenko, & Sargent 1997). *ASCA* and *BeppoSAX* observations find that the 2-10 keV luminosity of NGC 3998 is $\sim 3 \times 10^{41}$ erg s $^{-1}$ (Pellegrini et al. 2000; Terashima et al. 2002), and the 0.1-100 keV luminosity is $\sim 1 \times 10^{42}$ erg s $^{-1}$. The mass of a putative black hole in the nucleus of NGC 3998 is estimated to be $\sim 10^9 M_{\odot}$, giving $L_X/L_{Edd} \sim 1 \times 10^{-5}$, or well into the radiatively-inefficient accretion flow (RIAF) regime. The main goal of this paper is to contrast NGC 3998 with “normal” Seyfert 1 galaxies and to test the applicability of current RIAF models to the observed properties of NGC 3998.

We present the results of a recent *XMM-Newton* observation of NGC 3998, analyzed in conjunction with archival X-ray data. Previous X-ray observations showed that no Fe-K line is present in the X-ray spectrum from NGC 3998, and here we tighten this constraint, which places limits on the accretion geometry in NGC 3998. Additionally we will use *XMM-Newton* Optical Monitor data along with other multi-wavelength data to compare the spectral energy distribution (SED) of NGC 3998 with those predicted by various accretion models.

2. DATA REDUCTION

The parameters of X-ray observations are listed in Table 1. The *ASCA* data was reduced as described in Ptak et al. (1999) and Terashima et al. (2002). The *BeppoSAX* data were reduced by the XSELECT and FTOOLS in HEASOFT 5.2 from the cleaned event files obtained from the *BeppoSAX* Science Data Center. LECS and MECS spectra of NGC 3998 were extracted from a circular region with a 4 arcmin radius. Background spectra were taken from an annular region around NGC 3998. Here we present CCD spectra from the three EPIC detectors (two MOS and one PN) and the Optical Monitor U-band and UV (UVW2 filter) images. The *XMM-Newton* data was reduced using XMMSAS version 5.4.1 with the use of XAssist, a software package that performs the initial steps of X-ray data analysis (Ptak & Griffiths 2002). The XMM PN and MOS spectra were extracted from 37” circular regions (derived from fitting a Gaussian surface brightness model to the X-ray images). We compared the radial profile of the mos1 image (chosen since the target was not close to a ccd boundary in that case) to a SciSim simulation using the spectral model (see §3.1) and found that the X-ray emission from NGC 3998 is dominated by an unresolved source. The only other significant source in the vicinity of NGC 3998 is NGC 3998 X-1 (Roberts & Warwick 2000) which is discussed in §3.4. The OM data was reprocessed with XMMSAS and the images and source lists produced by the tool “omichain” were used in this paper. The OM spatial resolution depends on photon energy and the FWHM of the point-spread function (PSF) is 1.6” and 1.9” in the U and UVW2 bands (*XMM-Newton* User’s Guide). All spectra were binned to 20 counts/bin to allow the use of the χ^2 statistic.

3. RESULTS

3.1. Spectral Analysis

We fit the *XMM-Newton* (CCD) spectra of NGC 3998 with a simple absorbed power-law model, allowing the overall normalization of the model fit to each detector to be independent. This resulted in a good fit with $\Gamma \sim 1.9$, consistent with the previous *ASCA* and *BeppoSAX* observations as shown in Table 2. Note that while the three observations resulted in very close agreement for the power-law slope, the column density measurements varied from 3.3×10^{20} cm $^{-2}$ (or a factor of ~ 3 greater than the Galactic value; Murphy et al. 1996) to 8.0×10^{20} cm $^{-2}$. Given the calibration uncertainties below 0.5-1.0 keV for these detectors it is not clear to what extent these variations are significant. We show the power-law fit to the *XMM-Newton* data in Figure 1 (the *BeppoSAX* and *ASCA* data are plotted in Pellegrini et al. 2000 and Terashima et al. 2002). The *ASCA* data also resulted in a flux $\sim 30\%$ lower than the *BeppoSAX* and *XMM-Newton* measurements (see §3.3). Note that the PDS flux was $\sim 45\%$ higher the mean of the other flux measurements, however the bandpass of the PDS data was $\sim 10 - 100$ keV so the 2-10 keV flux is based on an extrapolation. We also tried restricting the *BeppoSAX* data to only include data below 10 keV (i.e., excluding the PDS data) and found no significant impact on the fit parameters. Power-law fit parameters from a fit to the *XMM-Newton* and *BeppoSAX* data simultaneously, with the normalization of each data set allowed to vary, is shown in Table 2, and χ^2 only increased by 3 when the normalization of the PDS component was fixed result in the same 2-10 keV flux as the MECS flux (i.e., the PDS data systematically deviate from the power-law fit at a confidence of only $\sim 90\%$).

There are no systematic residuals suggesting additional spectral features might be present. We do not find evidence for any edges suggesting that an ionized absorber is not present (note that the edges discussed in Pellegrini et al. were detected at less than the 3σ level). The RGS data do not have high enough signal-to-noise to constrain spectral features. There is a slight excess of counts in the 0.65-0.7 keV region but this feature is not statistically significant. We also tried a plasma plus power-law fit (Ptak et al. 1999) to the *XMM-Newton* spectra and found a significant improvement in χ^2 ($\chi^2/dof = 1406/1334$ compared with $1423/1338$ for the power-law fit). An absorption component applied to the whole spectrum resulted in $N_H = 4.6(1.0 - 5.8) \times 10^{20}$ cm $^{-2}$ and a separate absorbed applied to just the power-law component resulted in an upper limit of 4.9×10^{20} cm $^{-2}$. The temperature of the plasma component was 0.24 (0.18-0.43) keV, and the abundance was 0.016 (< 0.024). Note that the bulge velocity dispersion in NGC 3998 is 304 km s $^{-1}$ (McElroy 1995), implying a virial temperature of ~ 0.6 keV. Since NGC 3998 is an early-type galaxy and the inferred abundance from this fit is low, it is likely that this component is due to virial heating of the ISM (rather than starburst emission as is often observed in LLAGN). The power-law slope in this case was 1.84 (1.84-1.89), unchanged within the errors from the simple power-law fit. The thermal component obviously contributes to the spectrum most significantly at the lowest energies, with a 0.3-0.7 keV flux of 4×10^{-13} erg cm $^{-2}$ s $^{-1}$, or $\sim 13\%$ of the total 0.3-0.7 keV flux. However note that in this band the flux estimates of the 3 EPIC detectors differ by $\sim 8\%$ and therefore this component should be treated

TABLE 1. OBSERVATION PARAMETERS

Satellite	Bandpass (keV)	Date	Exposure Time (ks)
<i>ASCA</i>	0.4-10.0	05/10/94	40
<i>BeppoSAX</i>	0.1-100.0	06/29/99	24 (LECS), 77 (MECS), 38 (PDS)
<i>XMM-Newton</i>	0.2-10.0	05/09/01	12 (MOS), 9 (PN)

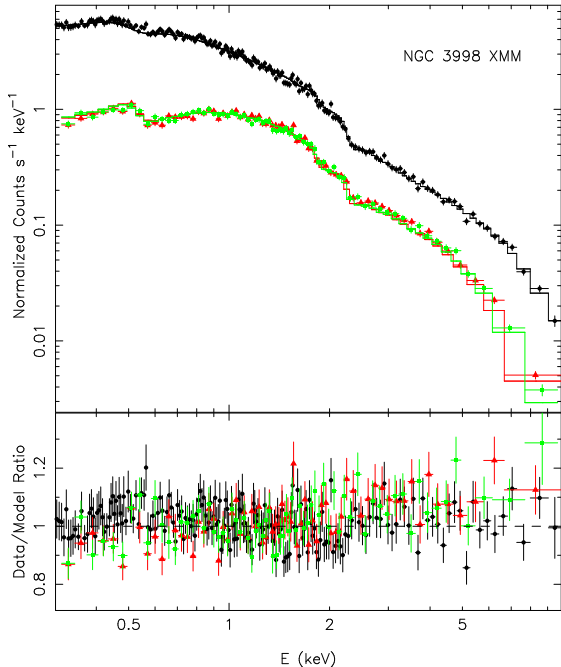


FIG. 1.— Power-law fit to the *XMM-Newton* spectra. The data and best-fitting model are shown in the top panel and the ratio of data to model is shown in the bottom panel. The PN, MOS1 and MOS2 data and residuals were marked with filled circles (black), filled triangles (red) and filled squares (green), respectively.

with caution.

In the *ASCA* GIS spectrum there is a small excess of counts near 6.4 keV which results in a “detection” of an Fe-K line. However the addition of a narrow Gaussian line ($\sigma = 0.01$ keV) to the *ASCA* power-law fit only reduces χ^2 by 3.7 (Terashima et al. 2002), which is only significant at a confidence of $\sim 96\%$ based on the f-test. In Table 3 we list the upper-limits obtained for narrow line emission with the energy fixed at 6.4 keV. Not surprisingly, the limit obtained when *ASCA* data is included in the fit is *higher* than when the *XMM-Newton* and *BeppoSAX* data are fit alone. In this table we list 90% errors for one interesting parameter ($\Delta\chi^2 = 2.7$), which are appropriate since here there is only one parameter of interest (the normalization of the line), however we also give $\Delta\chi^2 = 4.6$ errors for comparison with 2-parameter errors in the literature (or alternatively 97% 1-parameter errors). We also attempted to fit a disk line model (with the energy fixed at 6.4 keV, inclination fixed at 0° , power-law emissivity slope fixed at -2 and the inner and outer radii fixed at 5 and 500 in Schwarzschild units), and obtained upper-limits (for $\Delta\chi^2 = 2.7$) of 33 eV and 42 eV, without and with the *ASCA* data included, respectively.

3.2. Optical Monitor Data

The OM detector exposed five 1000 s images in the U and UVW2 filters, for a net exposure time of 5000 s in each band (additional exposures were taken of flanking fields which will not be discussed here). The central regions of the U and UVW2 images are shown in Figure 3. In order to properly model the surface brightness distributions for the two filters we also required model PSFs (there were no stars sufficient for this purpose in our observations). We initially produced model PSFs using SciSim. However, the current version of SciSim (3.0.0) does not specifically model the PSF-dependence of the individual filters, and also only models the PSF as a single Gaussian. Nevertheless, the resultant PSF FWHM was $\sim 2.1''$ which is similar to that expected for the UVW2 filter and therefore we proceeded with this PSF model for that filter. In the case of the U band filter we instead produced a model PSF by generating double Gaussian images and adjusting standard deviations of the two Gaussians and their relative normalization until the encircled energy function (i.e., the integrated radial profile) matched the values given in the OM calibration file OM_PSF1DRB_0006.CCF. In the surface brightness fitting described below we model the nuclear point-source component with a Gaussian whose standard deviation (σ) is permitted to be a free parameter. The fitted value of σ would then represent some combination of telescope jitter during the observation and also any adjustment to the PSF due to the inadequacies of our PSF model.

For UVW2 data, the XMMSAS tool “omichain” produces OM point source lists based on a $6''$ aperture and background taken from an aperture with radii 7-12". The nuclear 2120Å magnitude was 15.1 which corresponds to a flux density of 4.9×10^{-15} erg cm $^{-2}$ s $^{-1}$ Å $^{-1}$ (based on a Vega zero point and flux of 0.025 and 5.39×10^{-9} erg cm $^{-2}$ s $^{-1}$ Å $^{-1}$). The UVW2 images were fit with a double Gaussian model (with one Gaussian intended to represent any diffuse flux) from which it was determined that $\sim 50\%$ of the UV flux from NGC 3998 is extended over a $\sim 6''$ (FWHM) scale (the individual fits typically resulted in Gaussian σ values of $\sim 1''$ for the nuclear component and $\sim 3 - 4''$ for the diffuse component). Our spatial analysis implies that the flux density from within a $2''$ aperture was $\sim 2.5 \times 10^{-15}$ erg cm $^{-2}$ s $^{-1}$ Å $^{-1}$. Similarly, integrating the Gaussian fit for the nuclear component results in a count rate of ~ 0.5 counts s $^{-1}$, which implies a flux density of $\sim 2.4 \times 10^{-15}$ erg cm $^{-2}$ s $^{-1}$ Å $^{-1}$ (using a count rate to flux conversion factor of 4.871×10^{-15} erg cm $^{-2}$ s $^{-1}$ Å $^{-1}$ counts $^{-1}$ s). This result is in fairly good agreement with the values determined spectrally from IUE data in Reichert et al. (1992), 1.5×10^{-15} erg cm $^{-2}$ s $^{-1}$ Å $^{-1}$ and 1.2×10^{-15} erg cm $^{-2}$ s $^{-1}$ Å $^{-1}$ for the unre-

¹ all OM flux conversions discussed here are based on the calibration given at <http://xmm.vilspa.esa.es/sas/documentation/watchout/uvflux.shtml>

TABLE 2. POWER-LAW FITS TO X-RAY SPECTRA

Detector	N_H (10^{20} cm $^{-2}$)	Γ	F_{2-10} keV (10^{-11} erg cm $^{-2}$ s $^{-1}$)	χ^2/dof	Reference
<i>ASCA</i>	8.0 (6.9-9.2)	1.89 (1.86-1.92)	0.80	310.9/281	This work ¹
<i>BeppoSAX</i>	5.4 (3.5-7.8)	1.87 (1.83-1.90)	1.2	222.8/227	This work ²
<i>BeppoSAX</i> , <10 keV	5.1 (3.4-7.5)	1.86 (1.82-1.90)	1.1	207.9/210	This work
<i>XMM-Newton</i>	3.3 (3.0-3.6)	1.88 (1.87-1.90)	1.1	1422.6/1338	This work
<i>XMM-Newton</i> + <i>BeppoSAX</i>	3.3 (3.0-3.6)	1.88 (1.87-1.89)	1.1	1652.5/1567	This work

NOTE. — Errors are given in parenthesis for the 90% confidence interval assuming one interesting parameter (i.e., $\Delta\chi^2 = 2.7$).

¹See also Terashima et al. (2002)

²See also Pellegrini et al. (2000)

TABLE 3. FE-K EQUIVALENT WIDTH LIMITS

Detector(s)	EW, $\Delta\chi^2=2.7$	EW, $\Delta\chi^2=4.6$
<i>XMM-Newton</i>	< 32.7	< 41.4
<i>BeppoSAX</i>	< 38.2	< 56.0
<i>ASCA</i>	85.5 (11.7-159)	< 186
<i>XMM-Newton</i> + <i>BeppoSAX</i>	< 25 eV	< 33 eV
<i>XMM-Newton</i> + <i>BeppoSAX</i> + <i>ASCA</i>	< 33	< 40

NOTE. — In all fits the line energy and physical width were fixed at 6.4 keV and 0.01 keV (i.e., a narrow line), respectively.

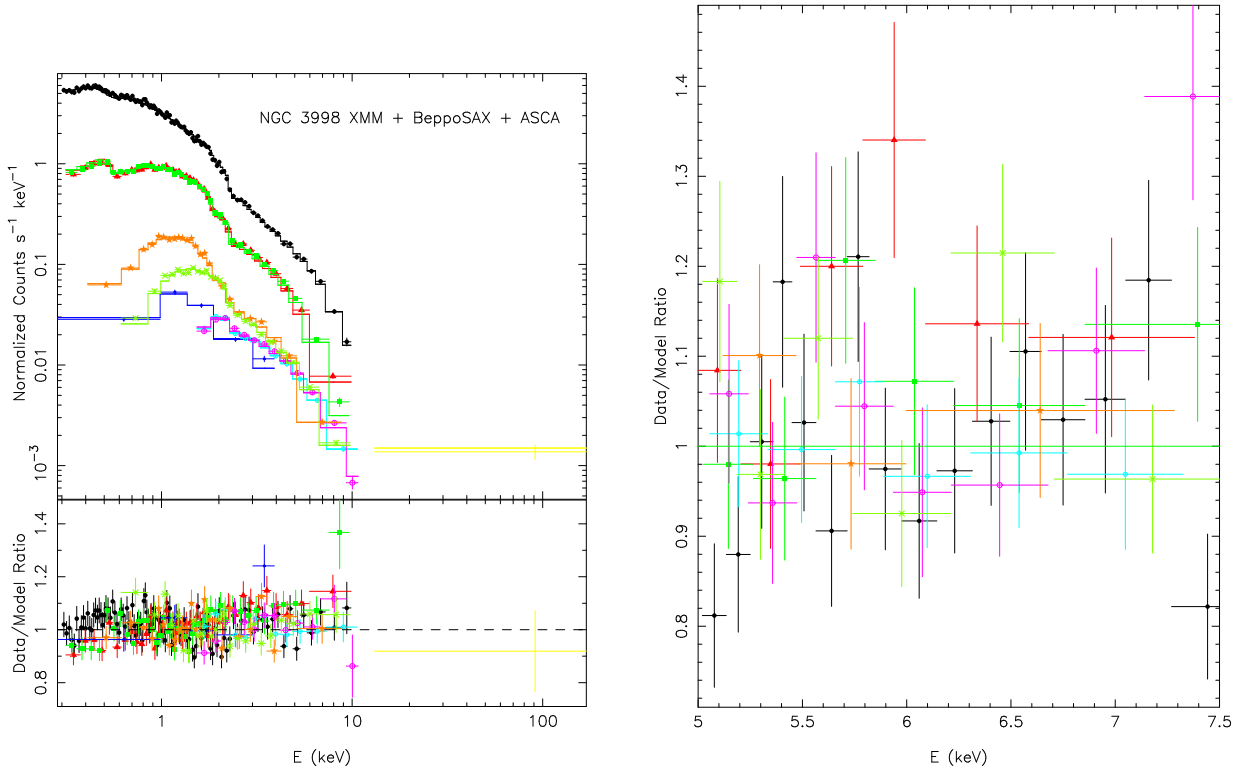


FIG. 2.— Power-law fit to the *XMM-Newton*, *BeppoSAX* and *ASCA* spectra. The normalization of each data set was allowed to vary independently. The column density of a cold absorber was allowed to vary independently for each observation (but was fixed to be the same for each *XMM-Newton* detector, for example). The data are marked as follows: *XMM* PN, MOS1, MOS2 = filled circles, filled triangles, and filled squares; *ASCA* SIS = filled star, GIS = crosses; *BeppoSAX* LECS, MECS2-3 = circles of increasing size, PDS = unmarked (the only data point beyond 10 keV). The data and best-fitting model are shown in the top panel and the ratio of data to model is shown in the bottom panel of the left plot, and the right plot shows only the data/model ratio in the 5.0-7.5 keV region.

solved and extended (FWHM $\sim 10''$) continuum components in the 1950-2155Å region. Given the uncertainties (particularly in the PSF model), we note that the actual nuclear flux density most likely lies in the range of $2.5 - 5.0 \times 10^{-15} \text{ erg cm}^{-2} \text{ s}^{-1} \text{ \AA}^{-1}$. We therefore assume a flux of $3.7 \times 10^{-15} \text{ erg cm}^{-2} \text{ s}^{-1} \text{ \AA}^{-1}$ with a 50% uncertainty. However, this value is a factor of $\sim 2 - 4$ lower than the FOC lower limit ($1.0 \times 10^{-14} \text{ erg cm}^{-2} \text{ s}^{-1} \text{ \AA}^{-1}$) determined by Fabbiano, Fassnacht, & Trinchieri (1994). Since the FOC UV data was overexposed in that observation our analysis will be based on the OM flux, and we note that it is possible that HST observed a flare in the UV bandpass.

The U band magnitude was determined from a $3''$ aperture (using the XMM-SAS tool “omsources” which allowed for smaller source radii in the case of U band images). The U band magnitude was 14.3, which corresponds to a flux of $6.1 \times 10^{-15} \text{ erg cm}^{-2} \text{ s}^{-1} \text{ \AA}^{-1}$ (with the Vega zero-point and flux being 0.025 and $3.16 \times 10^{-9} \text{ erg cm}^{-2} \text{ s}^{-1} \text{ \AA}^{-1}$ flux). The U band flux contains a contribution from the extra-nuclear emission but can of course nevertheless be considered to be an upper-limit to the nuclear U-band flux of NGC 3998. We fit the central images with a model that consisted of a Gaussian (again to represent a point source including jitter) and a de Vaucouleurs profile ($\propto \exp -7.669[(\frac{r}{r_e})^{1/4} - 1]$), where r_e is the scale length of the profile. These fits resulted in r_e values of $\sim 30 - 40''$, although the precise values are not particularly meaningful given the uncertainty in the PSF and the fact that we only fit the central $30''$ of the images since we are mainly interested in the determining the nuclear flux. The Gaussian σ values were $\sim 1.5''$, with the Gaussian component contributing 40-60% of the flux within a radius of $3''$. Here the count rate integrated from the nuclear Gaussian component is $\sim 11 \text{ counts s}^{-1}$, which results in a flux density of $2.1 \times 10^{-15} \text{ erg cm}^{-2} \text{ s}^{-1} \text{ \AA}^{-1}$. The U band HST FOC image was also overexposed, and Fabbiano, Fassnacht, & Trinchieri (1994) report a lower-limit of $4.2 \times 10^{-16} \text{ erg cm}^{-2} \text{ s}^{-1} \text{ \AA}^{-1}$ which is consistent with our flux.

The current flux calibration uncertainty for OM U and UV magnitudes is $\sim 10\%$ (U.S. XMM-Newton Guest Observer Facility, private communication). To check the calibration of the U band magnitudes, we computed the the (total) count rate of NGC 3998 and another galaxy in the U band FOV, NGC 3990, and derived U band magnitudes of 11.92 and 13.94. These values can be compared to the RC3 U band magnitudes of 12.13 and 13.81, respectively, or differences of 0.21 and 0.13. This implies that the flux calibration is indeed accurate to at least $\sim 10\%$. As with the UV flux, the nuclear U band flux the uncertainty is dominated by the contribution of the extra-nuclear component, and therefore we assume a value of $3.0 \times 10^{-15} \text{ erg cm}^{-2} \text{ s}^{-1} \text{ \AA}^{-1}$ (50% of the aperture photometry value) with a $\sim 30\%$ uncertainty (i.e., with 1σ being the offset to the model nuclear flux value discussed above).

In order to supplement the OM data with additional optical photometric points, we derived nuclear fluxes from the HST WFPC2 F547M (u2uh0505t, 200 second exposure) and F791W (u2uh0507t, 80 second exposure) observations of NGC 3998. For both images the net count rate was computed within a $0.1''$ circular aper-

ture (with the background estimated from an annulus at 2.5-2.6"). The count rates were converted to fluxes using the PHOTFLAM FITS keywords ($2.96 \times 10^{-18} \text{ erg cm}^{-2} \text{ s}^{-1} \text{ \AA}^{-1}$ and $7.69 \times 10^{-18} \text{ erg cm}^{-2} \text{ s}^{-1} \text{ \AA}^{-1}$ for F791W and F547M, respectively). This resulted in flux densities of $7.4 \times 10^{-16} \text{ erg cm}^{-2} \text{ s}^{-1} \text{ \AA}^{-1}$ and $7.9 \times 10^{-16} \text{ erg cm}^{-2} \text{ s}^{-1} \text{ \AA}^{-1}$ at 7872Å and 5484Å, respectively. We produced model PSFs for these images using TinyTim and fitted the central $3''$ (i.e., a 64×64 pixel image) with a Gaussian plus de Vaucouleurs model. This resulted in nuclear flux density estimates of $6.6 \times 10^{-16} \text{ erg cm}^{-2} \text{ s}^{-1} \text{ \AA}^{-1}$ and $7.6 \times 10^{-16} \text{ erg cm}^{-2} \text{ s}^{-1} \text{ \AA}^{-1}$, which do not differ by more than $\sim 10\%$ from values obtained above from aperture photometry, and we assume an error of 10% on these fluxes.

3.3. Variability

No statistically-significant short-term variability has been observed in the X-ray data, except for a marginally-significant, $\sim 12\%$ scale variation observed in the MECS data (Pellegrini et al. 2000). In Figure 4 we show the long-term 0.5-2.0 keV light curve of NGC 3998. These fluxes were derived from the ASCA, XMM-Newton, and BeppoSAX data discussed in this paper as well as archival ROSAT PSPC and HRI data (in which we converted the count rate to the 0.5-2.0 keV flux using a power-law with a slope of 1.88). The Einstein data point from 1979 is from Burstein et al. (1997) converted to the 0.5-2.0 keV bandpass. We chose 0.5-2.0 keV bandpass since it is within the energy ranges of these detectors, and, as shown in §3.1, there is a negligible contribution from hot gas to the spectrum (as would be expected since NGC 3998 is not a star-forming galaxy). From this plot, it appears that the flux of NGC 3998 was fairly constant during the measurements but may have been a factor of $\sim 50\%$ higher during the BeppoSAX and XMM-Newton observations. The Gina 2-10 keV flux for NGC 3998 was also high, by a factor of ~ 1.9 (~ 1.3) relative to the ASCA (BeppoSAX) fluxes, although it should be kept in mind that Gina was not an imaging telescope and had a FOV of $\sim 1^\circ$ (Awaki et al. 1991). Note that X-ray binaries are not expected to be a significant contributor to the X-ray luminosity of NGC 3998 since typical normal galaxy luminosities tend to be $\lesssim 10^{40} \text{ erg s}^{-1}$ (David, Jones, & Forman 1992), in contrast to $\sim 3 \times 10^{41} \text{ erg s}^{-1}$ for NGC 3998. More specifically, the B-band luminosity of NGC 3998 is $\sim 1.6 \times 10^{43} \text{ erg s}^{-1}$ (based on $B_T = 11.6$ from RC3), which implies a 0.5-4.5 keV luminosity of $\sim 1.6 \times 10^{39} \text{ erg s}^{-1}$ using the correlation in David, Jones, & Forman (1992).

3.4. NGC 3998 X-1

NGC 3998 X-1 (Roberts & Warwick 2000) is an extra-nuclear X-ray source just outside of the RC3 d_{25} ellipse of NGC 3998. In Figure 5 we show the PN image of the central $\sim 4'$ of NGC 3998 with the position of X-1 marked. X-1 was detected with 441, 73, and 84 net counts by the PN, MOS1 and MOS2 detectors, respectively, in $27.5''$ regions. Background spectra were extracted from circular regions of the same size in a source-free region away from the ULX and NGC 3998. A power-law fit resulted in $N_H = 0.5(< 5.7) \times 10^{20} \text{ cm}^{-2}$, $\Gamma = 1.8(1.6 - 2.1)$ and $\chi^2/\text{dof} = 25.9/32$ (see Figure 6). The 0.5-2.0 keV

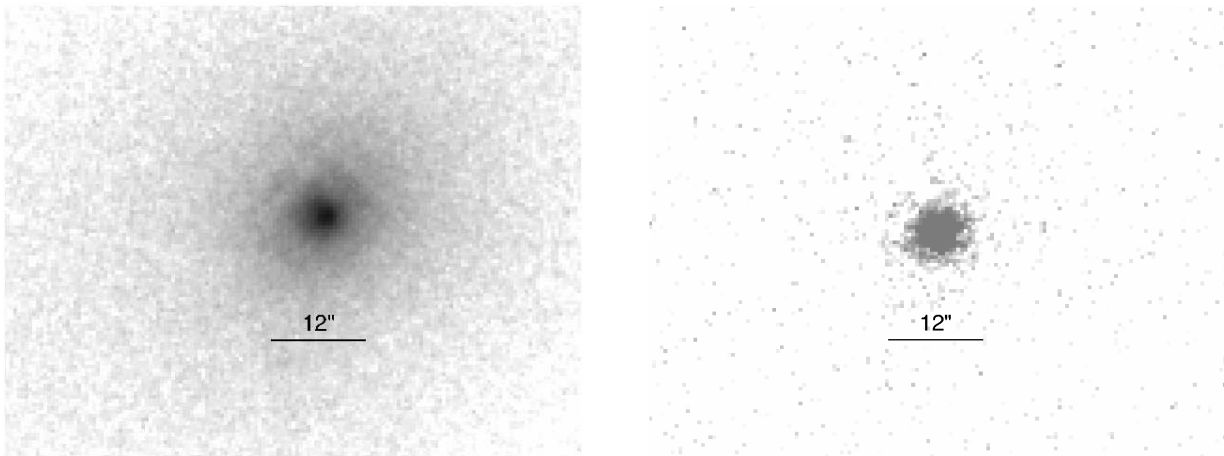


FIG. 3.— OM images of the central region of NGC 3998 in the U (left) and UVW2 (right) bands

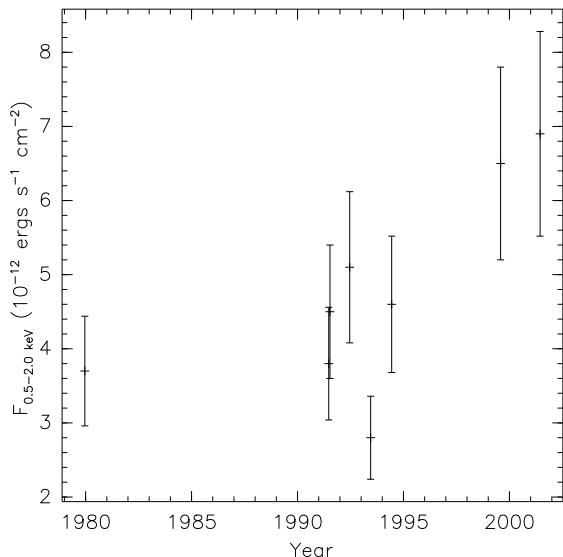


FIG. 4.— Long-term 0.5-2.0 keV light curve for NGC 3998 . All points are plotted with errors at the level of 20% ($\sim 2\times$ the variation in flux calibration typically observed between X-ray detectors. See Snowden (2002).

and 2-10 keV fluxes (averaged from the three detectors which differed from the mean by less than $\sim 25\%$) were $5.1 \times 10^{-14} \text{ erg cm}^{-2} \text{ s}^{-1}$ and $8.7 \times 10^{-14} \text{ erg cm}^{-2} \text{ s}^{-1}$. If this source is associated with NGC 3998 then the implied luminosity is $2 \times 10^{39} \text{ erg s}^{-1}$, making it an “ultra-luminous X-ray source” (ULX). A multi-color disk (MCD) black body model resulted in an unacceptable fit, with $N_H = 0. \text{ cm}^{-2}$, $kT_{in} = 0.7 \text{ keV}$, and $\chi^2/\text{dof} = 53.1/32$. The observed X-ray spectrum is consistent with ULXs, often observed with power-law spectra (e.g., Strickland et al. 2001; Foschini et al. 2002). However of course a power-law spectrum with $\Gamma \sim 1.9$ is also consistent with a background AGN. The *XMM-Newton* 2-10 keV logN-logS shown in Hasinger et al. (2001) implies that ~ 10 background sources deg^{-2} would be expected at this flux level or higher. X-1 is $1.6'$ from the nucleus NGC 3998, and so only ~ 0.02 background sources are expected at this flux or higher within this area, implying

that it is unlikely that this is a background source. Since we used a source-free region for the background spectra to avoid inaccurately subtracting flux due to NGC 3998 (as would result from using a “local” background), however the spectra of the ULX spectra then contain some contamination from NGC 3998. To quantify this, we used our SciSim simulation of the EPIC data and estimate that 0.19% of the flux of NGC 3998 is contaminating the X-1 source regions, or $\sim 2 \times 10^{-14} \text{ erg cm}^{-2} \text{ s}^{-1} = 24\%$ of the observed flux of X-1.

We also show in Figure 5 the U band image. After adjusting the astrometry by applying a $\sim 1''$ shift (derived by aligning the FIRST position of the nucleus of NGC 3998 and two USNO-B stars), an additional USNO-B source, 1454-0216445, is coincident with a U band source and NGC 3998 X-1. The U band source is detected with a signal-to-noise ratio of 9.3 and a magnitude 19.9 ± 0.3 (derived using the tool “omsource”; note that here the statistical error on the U magnitude is larger than the calibration uncertainties). The USNO-B 2nd epoch (1974.9) R and B magnitudes are 20.0 and 21.6. The USNO-B 1st epoch values are brighter by 0.5 and 0.7 magnitudes, respectively. However the uncertainty of USNO-B magnitudes is typically ~ 0.3 (Monet et al. 2003), and since these magnitudes are close to the flux limits of the survey ($V \sim 21$), their uncertainties are probably somewhat larger, particularly in the case of the B band magnitude. Therefore the difference between the two USNO-B epochs is probably just due to statistical fluctuation. Similarly the unusual “concave” spectrum implied by the USNO-B second epoch R and B magnitudes and the OM U band magnitude is largely due to the questionable B band magnitude.

4. DISCUSSION

As discussed in Pellegrini et al. (2000), the X-ray spectrum of NGC 3998 is fit well in the 0.1-100 keV bandpass with a simple power-law model that is only moderately absorbed ($N_H \sim 3 \times 10^{20} \text{ cm}^{-2}$ in contrast to the Galactic value of $\sim 1 \times 10^{20} \text{ cm}^{-2}$). We do not find any evidence for large-scale (i.e., $\Delta L/L > 25\%$) variability on short (< 1 day) time scales but NGC 3998 may have varied in the 0.5-2.0 keV bandpass on long time scales. Our main goal is to assess the physics of the accretion in NGC 3998,

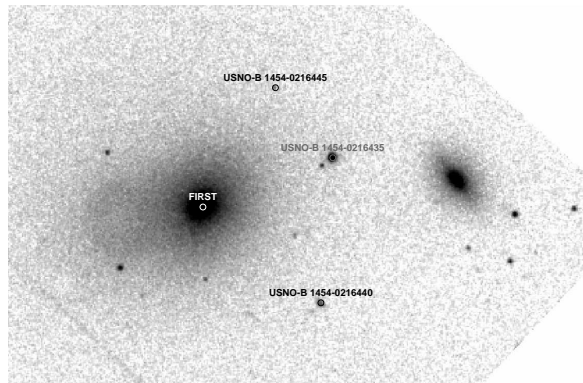
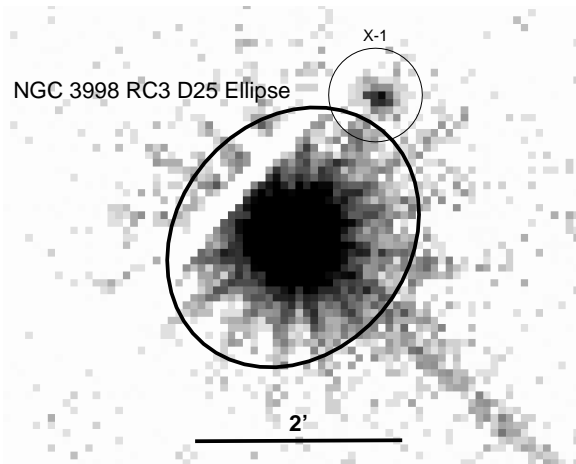


FIG. 5.— NGC 3998 PN (left) and U (right) images of NGC 3998. The PN image is marked with the RC3 d_{25} ellipse for NGC 3998 as well as the position of NGC 3998 X-1. The U band image shows the FIRST position for NGC 3998 along with USNO-B 1454-0216435 and USNO-B 1454-0216440 after shifting by $\sim 1''$ in order to align with the nucleus of NGC 3998 and two stars in the field. Also shown is the position of USNO-B 1454-0216445 which aligns with a U band source that may be associated with NGC 3998 X-1. The *XMM-Newton* X-ray position for X-1 is $11^{\circ}57^m50^s, 55^h28^m34^s$ J2000. The position of USNO-B 1454-0216445 is $11^{\circ}57^m50.27^s, +55^h28^m34.9^s$ (offset $2.1''$ from the X-ray position).

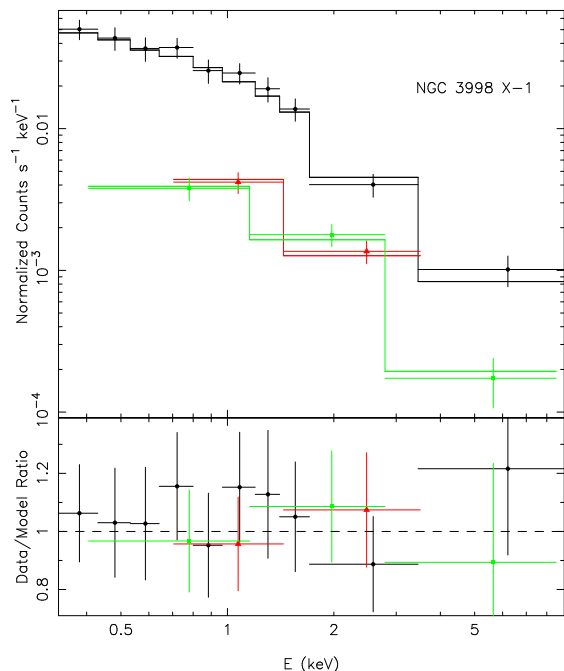


FIG. 6.— Power-law fit to the PN, MOS1 and MOS2 data (marked with filled circles, triangles, and squares, respectively) for NGC 3998 X-1.

and below we compare these observed X-ray properties of NGC 3998 with those observed in other AGN, and compare the SED of NGC 3998 with Seyfert 1 and RIAF models. We also speculate on the constraints that our results can place on the geometry of the nucleus of NGC 3998.

4.1. Comparison with Seyferts

The presence of broad $H\alpha$ in NGC 3998 suggests that the nuclear region might be similar in structure to “typical” Seyfert 1 galaxies. The X-ray slope of NGC 3998 ($\Gamma = 1.9$) is consistent with typical Seyfert

1 galaxies, and the 2-10 keV luminosity of NGC 3998 (2.6×10^{41} erg s^{-1} for $F_{2-10 \text{ keV}} = 1.1 \times 10^{-11}$ erg $cm^{-2} s^{-1}$) is only marginally low for typical Seyfert galaxies (Nandra, George, Mushotzky, Turner, & Yaqoob 1997a). However, NGC 3998 differs in two important respects from typical Seyfert 1 galaxies. First, the lack of strong X-ray variability is in contrast with typical Seyferts, particularly on short time scales, since the trend there is for variability to increase with decreasing luminosity (Nandra, George, Mushotzky, Turner, & Yaqoob 1997a). Ptak et al. (1998) suggested that this is typical of LINERs and LLAGN (including NGC 3998) and that the X-ray source regions are larger in LINERs and LLAGN than in typical Seyferts. One possibility is that the X-ray production is occurring in optically-thin flows (see below) rather than flares in optically-thick accretion disks.

The X-ray spectrum is also remarkably featureless in contrast with typical Seyfert 1 galaxies, particularly with the lack of any Fe-K emission at 6.4 keV. The upper-limit to the equivalent width (EW) in the *XMM-Newton* and *BeppoSAX* joint fit is 25 eV. Figure 7 shows the distribution of narrow-line EWs measured in a sample of Seyfert 1 galaxies (Nandra, George, Mushotzky, Turner, & Yaqoob 1997c), where we also show the upper-limit for NGC 3998. The trend in Seyfert 1s is to have higher EW Fe-K lines with decreasing luminosity, and accordingly the lack of a line in NGC 3998 is conspicuous. A cautionary point is that Figure 7 is based on Seyfert 1s with Fe-K lines and does not account for Seyfert 1s lacking Fe-K lines. However, the vast majority of (X-ray bright) Seyfert 1 galaxies appear to exhibit some level of Fe-K emission (Nandra, George, Mushotzky, Turner, & Yaqoob 1997b), with very few Seyfert 1s being known that lack a Fe-K line when the spectra are of sufficient quality for Fe-K emission to be detected (T. Yaqoob, priv. comm.). Thus, it is likely that the accretion physics and/or geometry in NGC 3998 differs somewhat from typical Seyfert 1 galaxies.

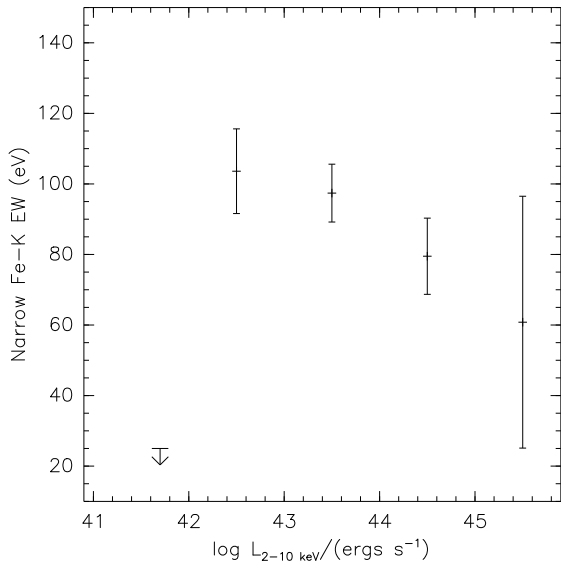


FIG. 7.— Observed narrow-line Fe-K EWs as a function of luminosity for Seyfert 1 galaxies from Nandra, George, Mushotzky, Turner, & Yaqoob (1997c) with the upper-limit for NGC 3998 also shown.

4.2. Radiatively-Inefficient Accretion Flows

By integrating the best-fitting power-law to the *XMM-Newton* and *BeppoSAX* data ($\Gamma = 1.88$ with normalization 3.8×10^{-3} photons $\text{keV}^{-1} \text{cm}^{-2} \text{s}^{-1}$) we calculate the unabsorbed 0.1-100 flux to be $6.4 \times 10^{-11} \text{erg cm}^{-2} \text{s}^{-1}$, or a luminosity of $\sim 1.5 \times 10^{42} \text{erg s}^{-1}$. Using the bulge velocity dispersion of 304km s^{-1} from McElroy (1995) and the bulge dispersion/black hole mass relation given in Tremaine et al. (2002) we estimate the black hole mass of NGC 3998 to be $\sim 7 \times 10^8 M_{\odot}$. This implies an Eddington luminosity ($L_{Edd} = 1.25 \times 10^{38} \frac{M}{M_{\odot}}$) of $9 \times 10^{46} \text{erg s}^{-1}$, so $L/L_{Edd} = 2 \times 10^{-5}$ (note that we get a similar result if we use the typical LLAGN ratio of $L_{2-10 \text{ keV}}/L_{bol} = 0.15$ found by Ho [1999]). One possibility is that the low luminosities in NGC 3998 are reflecting low accretion rates. Recent accretion modeling suggests that at low accretion rates (\lesssim a few percent of the Eddington rate; see Narayan, Mahadevan, & Quataert 1998) the flow will have low particle densities, and in turn may be optically thin and radiatively inefficient. In general these models predict that the X-ray spectrum from an RIAF is dominated by inverse-Compton scattering (of synchrotron emission) and results in somewhat steep X-ray slopes (as opposed to the flat slopes expected from bremsstrahlung emission, e.g., see Mahadevan 1997). For example, in the case of convection-dominated accretion flows (CDAFs), X-ray slopes of ~ 2 are expected when $L_X/L_{Edd} > 10^{-7}$ (Ball, Narayan, & Quataert 2001). The X-ray temporal and spectral properties of NGC 3998 described above are similar to other LINERs thought to contain RIAFs (e.g., Ptak et al. 1998; Quataert et al. 1999) (although again the X-ray spectral slope is consistent with typical Seyfert 1s also).

4.3. Spectral Energy Distribution

We turn now to comparison of the SED of NGC 3998 to the predictions of various models. The data used to derived the SED of NGC 3998 is listed in Table 4 and

is shown in Figure 8. The X-ray data shown has been “unfolded” to remove the spectral response of the detectors and have been binned more so than in Figure 2 for display purposes. The points marked with open circles can be considered to be upper-limits since they are sampling radii $> 10''$. In the near-IR the large aperture points are clearly dominated by galactic emission (and accordingly the small aperture points contain a large contribution from galactic light). However in the radio to mid-IR region the radiation appears to be fairly compact (i.e., unresolved to aperture sizes less than $\sim 10''$, see also Knapp et al. 1996). Also variability is evident among several of the radio and (possibly also) mid-IR measurements listed in Table 4, which also implies that the emission is compact. Note that SEDs for NGC 3998 were also presented in Fabbiano, Fassnacht, & Trinchieri (1994) and Pellegrini et al. (2000), however those papers assume the HST FOC UV flux, which is a factor of $\sim 2 - 4$ higher than our OM measurement. This higher UV flux results in a SED that resembles a typical AGN, while our lower UV flux results in a SED more consistent with the sample of low-luminosity AGN discussed in Ho (1999). It is also evident that in the optical band, only the HST data with $\sim 0.1''$ apertures are sufficient to exclude large contributions of extra-nuclear flux. Given the large low-mass star contribution to near-IR emission of early-type galaxies, this is also true for the near-IR band. The relative amounts of flux in the OM U band and HST FOC U band suggests that this contribution is at least 90%, and likely to be much larger at longer wavelengths.

We assessed the impact of extinction using the extinction equations in Cardelli, Clayton & Mathis (1989). Knapp, van Driel, & van Woerden (1985) found that the upper-limit for HI absorption to the nucleus of NGC 3998 was $\sim 4 \times 10^{20} \text{cm}^{-2}$. Including the Galactic contribution of $\sim 1 \times 10^{20} \text{cm}^{-2}$ results in a conservative estimate of $N_H \sim 5 \times 10^{20} \text{cm}^{-2}$. This value is consistent with the X-ray observations here with the exception of the *ASCA* data, however again we note that the calibration of the low energy response of the *ASCA* CCD detectors is somewhat uncertain. This corresponds to $A_V \sim 0.22$ (Jenkins & Savage 1974), and from Cardelli, Clayton & Mathis (1989) we derive that $\sim 50\%$, 30% and 25% of the flux at UVW2, U and B, respectively, would be absorbed. This level of extinction does not impact our conclusions.

Comparison with RIAF Models

For accretion onto a black hole, the gravitational in-fall timescale can be shorter than the radiative timescale; the accretion energy is then stored as thermal energy instead of being radiated (e.g., Rees et al. 1982; Narayan & Yi 1994). In the past few years, analytical and numerical work has shown that the physics of such RIAF models is far more complex than originally anticipated. In particular, very little mass available at large radii actually accretes into the black hole; most of it is lost to an outflow (i.e., in an adiabatic inflow/outflow solution, or “ADIOS”) or circulates in convective motions (e.g., Blandford & Begelman 1999; Stone, Pringle, & Begelman 1999; Igumenshchev & Abramowicz 2000; Quataert & Gruzinov 2000; Hawley & Balbus 2002; Ballantyne & Ross 2002). The accretion of slightly rotat-

TABLE 4. LUMINOSITY DATA FOR NGC 3998

ν (Hz)	νL_ν ($ergs\ s^{-1}$)	Aperture ($''$)	Reference
3.2×10^8	6.5×10^{36}	60	Rengelink et al. (1997)
6.0×10^8	1.4×10^{37}	30	Hummel, van der Hurst, & Dickey (1984)
1.4×10^9	3.3×10^{37}	24	Hummel (1980)
1.4×10^9	3.4×10^{37}	45	Condon et al. (1998)
1.4×10^9	3.1×10^{37}	5	FIRST
2.7×10^9	7.0×10^{37}	6	Condon & Dressel (1978)
5.0×10^9	9.1×10^{37}	0.5	Hummel, van der Hurst, & Dickey (1984)
5.0×10^9	1.0×10^{38}	0.008	Hummel et al. (1982)
5.0×10^9	9.6×10^{37}	0.007	Filho, Barthel, & Ho (2002)
8.1×10^9	1.8×10^{38}	6	Condon & Dressel (1978)
1.5×10^{10}	2.1×10^{38}	0.1	Hummel, van der Hurst, & Dickey (1984)
3.0×10^{12}	8.6×10^{41}	180	IRAS
5.0×10^{12}	6.6×10^{41}	90	IRAS
1.2×10^{13}	3.7×10^{41}	45	IRAS
1.5×10^{13}	1.0×10^{42}	8	Willner et al. (1985)
2.5×10^{13}	8.4×10^{41}	45	IRAS
3.0×10^{13}	2.1×10^{41}	8	Willner et al. (1985)
3.0×10^{13}	3.8×10^{41}	6	Willner et al. (1985)
3.0×10^{13}	3.7×10^{41}	6	Willner et al. (1985)
8.6×10^{13}	1.5×10^{42}	5	Willner et al. (1985)
1.4×10^{14}	5.5×10^{42}	3	Alonso-Herrero et al. (2000)
1.4×10^{14}	4.0×10^{42}	5	Willner et al. (1985)
1.4×10^{14}	5.1×10^{42}	11	Longmore & Sharples (1982)
1.4×10^{14}	8.3×10^{42}	15	Frogel et al. (1978)
1.4×10^{14}	4.0×10^{42}	4	2MASS Point Source Catalog
1.8×10^{14}	6.8×10^{42}	5	Willner et al. (1985)
1.8×10^{14}	9.0×10^{42}	11	Longmore & Sharples (1982)
1.8×10^{14}	1.4×10^{43}	15	Frogel et al. (1978)
1.8×10^{14}	6.4×10^{42}	4	2MASS Point Source Catalog
2.5×10^{14}	9.0×10^{42}	3	Alonso-Herrero et al. (2000)
2.5×10^{14}	7.8×10^{42}	5	Willner et al. (1985)
2.5×10^{14}	9.9×10^{42}	11	Longmore & Sharples (1982)
2.5×10^{14}	1.5×10^{43}	15	Frogel et al. (1978)
2.5×10^{14}	7.4×10^{42}	4	2MASS Point Source Catalog
3.8×10^{14}	1.3×10^{41}	0.1	This work
5.5×10^{14}	1.0×10^{41}	0.1	This work
5.9×10^{14}	1.6×10^{41}	0.1	Fabbiano, Fassnacht, & Trinchieri (1994)
8.7×10^{14}	2.5×10^{41}	3	This work
8.8×10^{14}	$>5.5 \times 10^{40}$	0.1	Fabbiano, Fassnacht, & Trinchieri (1994)
1.4×10^{15}	1.8×10^{41}	2	This work
1.8×10^{15}	$>4.1 \times 10^{41}$	0.1	Fabbiano, Fassnacht, & Trinchieri (1994)

ing gas also may result in a substantially reduced accretion rate relative to the Bondi rate (Proga & Begelman 2003). Following a proposal due to Blandford & Begelman (1999), we can parameterize the radial variation of the gas density in the flow with a parameter p , where $\rho \propto r^{-3/2+p}$ (equivalently, the accretion rate varies with radius as $\dot{m} \propto r^p$); $p \approx 1/2 - 1$, rather than $p = 0$ (as in the original analytical advection-dominated accretion flow [ADAF] models of Narayan & Yi 1994), is favored by the simulations, implying much lower gas densities close to the black hole.

Figure 8a shows several RIAF models for the SED of NGC 3998. Quataert & Narayan (1999) showed that there are significant degeneracies in comparing theoretical RIAF spectra to observed data so these results should be interpreted as representative models, not unique “fits.” The solid line in 8a is an ADAF with an accretion rate of 3×10^{-3} (hereafter accretion rates are given in Eddington units) and $\delta = 0.01$ (= fraction of the accretion energy transferred to electrons). The dotted line is the ADAF model with an outer thin disk starting at a transi-

tion radius $r_t = 300R_s$ (R_s = the Schwarzschild radius). The dot-dashed line is an ADIOS model with $\delta = 0.3$ and $p = 0.4$ and a similar accretion rate at the outer edge of the flow, also with an outer thin disk (the so-called multi-color disk (MCD) model) with $r_t = 300R_s$. Note that ADIOS models result in similar spectral models to CDAF models. The thin disk (for both models) has an outer radius of $10^5 R_s$, an inclination of 60 degrees, and $\dot{m} \approx 3 \times 10^{-3}$ (hereafter all \dot{m} values are quoted in Eddington units). Given theoretical uncertainties about electron heating, values of $\delta \ll 1$ to $\delta \sim 1$ are plausible (e.g., Quataert & Gruzinov 1999), and the two models chosen in fact span this range. These models fit the IR-X-ray emission reasonably well, except of course for the large contribution of stellar flux at near-IR wavelengths. The (nuclear) IR emission is dominated by the (putative) thin disk component while the UV-X-rays are dominated by the RIAF, and in fact r_t and the accretion rate at r_t were chosen to approximately match the IR flux. The smaller r_t value could have been chosen which would have resulted in a larger thin-disk flux, and correspondingly a

smaller \dot{m} would have been chosen. Therefore the values of \dot{m} and r_t are only constrained to within \sim an order of magnitude. The X-ray emission in these RIAF models is dominated by inverse-Compton scattering which results in approximately in a power-law continuum. The ADIOS model has a lower \dot{m} and density near the black hole, but a larger temperature. In that situation, the Compton peaks are more 'separated' (since the energy gain per scattering is proportional to temperature) and the peaks are more distinct. This is a generic difference between high \dot{m} ADAF type models and lower \dot{m} models. Since the X-ray spectrum of NGC 3998 is fairly featureless lower temperature models are more consistent with the X-ray data. Note that in general different thermal line emission characteristics are predicted for these different types of models, but these lines are not detectable at this \dot{m} (Perna, Raymond, & Narayan 2000). Neither model accounts for the radio emission, in spite of the fairly large outer disk radius of $10^5 R_s$. The most restrictive constraint in this regard is the VLBI 5 GHz point which has a beam size of only 7 mas, or ~ 0.7 pc, and is clearly nuclear in origin.

AGN Spectral Models

In Figure 8b we also plot the median SEDs for radio-loud and radio-quiet AGN from Elvis et al. (1994), rescaled to the flux of NGC 3998 at $\nu = 10^{18}$ Hz. The QSO SEDs grossly overestimate the blue-UV emission, i.e., NGC 3998 is lacking the "big blue bump" that is considered to be due to an optically-thick accretion disk. However, this is not unexpected since the accretion rate is much lower than that of a typical QSO, and MCD temperatures scale as $\dot{m}^{1/4}$ (Frank, King, & Raine 2002). We also show an approximate Comptonized thin-disk model that fits the X-ray data from NGC 3998 without over-predicting optical or IR flux. This thermal Comptonization model (implemented in XSPEC as "compTT"; see Titarchuk 1994, Hua & Titarchuk 1995) uses the Wien approximation to black body flux for computational efficiency, however this should be a reasonable approximation. In this model there are 5 parameters: the overall normalization, the temperature of the Wien component, the temperature and optical depth (τ) of the hot plasma, and a geometry switch to select a spherical or disk geometry. In general inverse-Compton spectra tend to be power-laws with a slope of $-\frac{\ln \tau}{\ln A}$, where A is the mean amplification of the photon energy per scattering (Rybicki & Lightman 1979). Therefore it is not surprising that for a given Wien and plasma temperature combination, τ could be adjusted to result in our observed power-law slope and hence give a good fit. The fits generally resulted in a power-law extrapolated from the peak of the Wien component, and we therefore initially fixed the temperature of the Wien spectrum at 10^{-4} keV ($\sim 10^3$ K) to see if the power-law could be extended to the optical bandpass. We tried hot plasma temperatures of 100 and 200 keV (see Pietrini & Krolik 1995), and fitted for the model normalization and τ as free parameters. The best-fit optical depths were 0.3 and 0.1 for a disk geometry and plasma temperatures of 100 and 200 keV, respectively. With a spherical geometry the best-fit optical depths were 0.5 and 1.0 for plasma temperatures of 100 and 200 keV. Clearly the value of τ is not meaningful since our data do not constrain the geometry or tempera-

ture of the hot plasma. These fits (simultaneously to the *XMM-Newton* and *BeppoSAX* data) resulted in $\chi^2/\text{dof} = 1653-1654/1567$, or basically equivalent to the pure power-law fit. The fit with a plasma temperature of 200 keV and a disk geometry is shown in Figure 8. We computed a MCD spectrum (with inner radius = $3R_s$ and outer radius = $10^5 R_s$) consistent with the Wien component by assuming an inclination angle of 60 degrees and adjusting \dot{m} , which resulted in $\dot{m} = 4.1 \times 10^{-6}$. Such a model accounts for the spectrum of NGC 3998 from the optical to ~ 100 keV, i.e., the optical flux is consistent with the extrapolation of the power-law observed in the X-ray band, particularly if we allow for variability in the FOC F480LP flux (the offset between the PDS point in Figure 8 and the Comptonized spectrum model is due in part to the fact that the X-ray data were unfolded assuming the simple power-law spectrum extending to 100 keV). However this model requires that a *negligible* fraction of the emission longward of the optical is due to the AGN in NGC 3998. This may be unlikely given the compactness of the radio and mid-IR emission.

Of course there is some degeneracy between the inclination angle and accretion rate of the disk in this scenario, with an angle of 0° and $\dot{m} = 2.0 \times 10^{-6}$ also being consistent with the Wien component. However the luminosity of the MCD disk component is not arbitrary. The MCD spectrum is given by the sum of blackbody spectra with temperatures varying as $r^{-3/4}$ where r is radius of each point on the surface of the disk (Frank, King, & Raine 2002). This results in a spectrum similar to a single blackbody emitting at the peak temperature of the disk, and for given black hole mass the peak temperature scales as $\dot{m}^{1/4}$. Of course the luminosity of a blackbody emitting over a given surface area is proportional to ν^4 , where $h\nu \sim 3kT$. Therefore we could not match the luminosity of the MCD component for other disk temperatures by simply adjusting the accretion rate since the expected luminosity of the Wien component would move in the $\log L_\nu - \nu$ plane along a slope of 4 rather than 0.9. This makes the Comptonized MCD model inconsistent with the observed X-ray power-law if the peak disk temperature is below $\sim 10^{-4}$ keV (i.e., the Wien component normalization would be larger than the MCD expectation), and also at higher temperatures this model is only consistent with the data if the MCD component is attenuated (e.g., by inclination effects). Also note that the optical (UV) flux would not be due to the accretion disk for disk temperatures in excess of $\sim 10^{-4}(10^{-3})$ keV. Conversely, assuming that the optical and UV data are due to a thin disk requires that $\dot{m} \lesssim 10^{-5}$. Finally, note that a standard α disk is both stable and optically thick when \dot{m} is in the range discussed here ($10^{-6} < \dot{m} < 10^{-5}$).

Jet Models

In addition to a very low accretion rate, another possibility is that both the radio and X-ray flux from NGC 3998 are due to a jet, as has been suggested recently for LLAGN such as NGC 4258 (Yuan et al. 2002), IC 1459 (Fabbiano et al. 2003) and NGC 4594 (Pellegrini et al. 2003). Along these lines we show a simple broken power-law model in Figure 8, where we found that the radio data were consistent with a slope of ~ 0 (i.e., with $\nu L_\nu \propto \nu^1$) and break frequency of $\sim 10^{12}$ Hz. This is

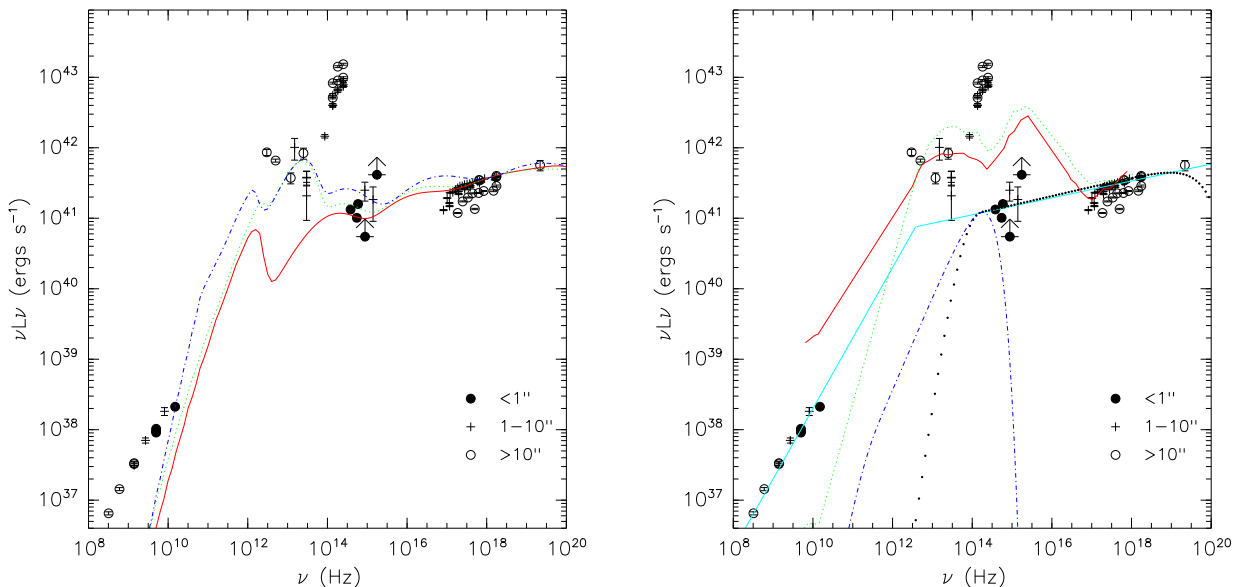


FIG. 8.— The SED of NGC 3998 plotted with (left panel) two RIAF models and (right panel) the radio-load (red solid line) and radio-quiet (green dotted line) mean QSO SEDs from Elvis et al. (1994). The U and UV points (at $\nu \sim 10^{15}$) are due to the OM, and the X-ray points are due to the spectral fits discussed in the text (note that the data points have been “unfolded” to account for the spectral responses of the detectors and hence are somewhat model dependent). The turn-over in the X-ray data at low energies is due to absorption (with $N_H \sim 3 \times 10^{20} \text{ cm}^{-2}$). The X-ray data points with lower luminosities are due to *ASCA* (see text). The RIAF models are computed with an inner ADAF (green dotted line; $\dot{m} = 3 \times 10^{-3}$ in Eddington units, $\delta = 0.01$) and an inner ADIOS (blue dot-dashed line; $\dot{m} = 3 \times 10^{-3}$, $\delta = 0.3$, $p = 0.4$), both with an outer thin disk with a transition radius of $300 R_s$ and outer radius of $10^5 R_s$. We also plot the ADAF model with no outer thin disk for comparison (red solid line). The right panel also shows a Comptonized disk spectrum (black bold dotted line). The Comptonization model used is based on a Wien spectrum approximation, and we show the equivalent multi-color disk model for comparison (blue dot-dashed line; the parameters were $\dot{m} = 4.1 \times 10^{-6}$, and inclination angle = 60°). A simple broken power-law model with a radio slope of 0.0 and an IR-to-Xray slope of 0.9 is also shown in the right panel as a representative synchrotron model.

obviously an overly simplistic model but here the radio slope is due to optically-thick synchrotron emission and the X-ray emission is due to optically-thin synchrotron emission, modeled by Markoff, Falcke, & Fender (2001) as being due to the outer, “post-shock” portion of the jet. The Markoff-Falcke model also predicts a mid-IR “bump” due to synchrotron emission from the inner, “pre-shock” jet which may be consistent with the mid-IR fluxes observed in NGC 3998. Alternatively, the synchrotron emission may break to a flatter slope and the X-ray is again also due to inverse-Compton emission, and the mid-IR and/or optical-UV flux is due to a standard α disk (Markoff et al. 2003). Clearly these models would also be consistent with the SED of NGC 3998 and may imply accretion rates possibly orders-of-magnitude higher than the RIAF and Comptonized α -disk models since a large fraction of the accretion energy would be released kinetically in the jet. However, as was the case in the SED modeling discussed above, any α disk in this scenario would likely still need to be truncated to avoid over-predicting the optical and UV fluxes. Also, the lack of any short-term, large-amplitude X-ray variability may argue against the X-ray emission being dominated by a (relativistic) jet.

4.4. Constraints on the Nuclear Geometry of NGC 3998

The Fe-K lines in Seyfert 1 galaxies are assumed to originate from reflection from a thin disk and/or matter further out such as the putative “torus” in the standard model (Yaqoob & Padmanabhan 2002). If the Fe-K emission is dominated by a thin disk, then the maxi-

mal solid angle as seen from the X-ray source would be $\sim 2\pi$, and the solid angle of a toroidal geometry of matter most likely would not exceed this. If we assume that the EW ~ 100 eV Fe-K line typically observed in Seyfert 1 galaxies is produced by a reflection from optically-thick material with $\Omega \sim 2\pi$, then our upper-limit of ~ 25 eV implies that $\Omega/2\pi \sim 0.25$ in NGC 3998. Interestingly, Pellegrini et al. (2000) report a similar result of $\Omega/2\pi < 0.21$ for either a neutral or ionized Compton reflection hump based on reflection model fits to the *Bep-poSAX* spectrum of NGC 3998. We also computed an upper-limit for a disk line model at 6.4 keV and obtained ~ 30 eV. A $L_{2-10 \text{ keV}} = 10^{42} \text{ erg s}^{-1}$ Seyfert 1 would typically exhibit a EW = 300 eV disk line, which implies $\Omega/2\pi < 0.1$. This suggests that the solid angle of *any* optically-thick material in NGC 3998 is less than at most 25% of that typically observed in Seyfert 1 galaxies.

We can roughly constrain the size of an outer thin disk using the line information. Assuming a disk geometry with the X-ray source at a height h above the center of the disk with inner and outer radii r_{in} and r_{out} , the solid angle subtended by the disk is given by $\Omega = 2\pi[(1 + (\frac{r_{in}}{h})^2)^{-1/2} - (1 + (\frac{r_{out}}{h})^2)^{-1/2}]$. The X-rays are produced in the inner part of the RIAF, implying $h \sim 10 - 30 R_s$. It is therefore likely that $r_t \gg h$. This implies that $\frac{\Omega}{2\pi} \sim h(\frac{1}{r_{in}} - \frac{1}{r_{out}})$ and therefore $r_t \gtrsim \frac{h}{\frac{\Omega}{2\pi}}$, or $r_t \gtrsim 100 - 300 R_s$ for $\frac{\Omega}{2\pi} \lesssim 0.1$. This is consistent with Figure 8 where we assumed $r_{in} = r_t \sim 300 R_s$. A possible caveat to this analysis is that NGC 3998 may contain an optically-thick disk with $r_{in} = 3 R_s$ but whose surface layers are fully

ionized. This could result in little or no Fe-K emission (Done & Nayakshin 2001; Ballantyne & Ross 2002).

4.5. The Nature of the ULX NGC 3998 X-1

If this source is associated with NGC 3998, then the optical luminosity of the source ($M_R \sim -11$) implies several to tens of supergiant stars or a cluster of hundreds to thousands of low-mass stars, if the optical flux is stellar. If the optical variability observed between the two USNO-B epochs (separated by of order 25 years) were real it would argue against this, although again the variability is probably not statistically significant. In addition, the high U-band absolute magnitude ($M_U = -10.9$) and very blue color imply that any such cluster would be composed of early-type stars. This rules out a globular cluster with late-type stars which would be expected in an early type galaxy. Using $\log F_X/F_{opt} = \log(F_{0.5-2.0 \text{ keV}}) + R/2.5 + 5.7$ (Honschmeier et al. 2003; Szokoly et al. 2004; Norman et al. 2004), we derive $\log F_X/F_{opt} = 0.4$ for the ULX which is typical of AGN found in the CDFS (Szokoly et al. 2004; Norman et al. 2004) and is much larger than values typical of stars ($\log F_X/F_{opt} \ll -1$) and somewhat smaller than values typical of low-mass X-ray binaries ($\log F_X/F_{opt} > 1$; Bradt & McClintock 1983; although realistically we would be observing an X-ray binary in a cluster). The most likely identification for this source is therefore a background AGN, although as stated in §3.4, the detection of a background source at this flux was unlikely.

5. SUMMARY

We have determined the tightest constraint to date on Fe-K emission in NGC 3998, specifically $EW < 25 \text{ eV}$ for a narrow line at 6.4 keV. Our analysis of *XMM-Newton* data combined with archival *ASCA* and *BeppoSAX* data shows that the spectrum is fit well with a simple power-law with $\Gamma = 1.9$ and a small amount of intrinsic absorp-

tion. The *XMM-Newton* OM UV flux measurement is consistent with an extrapolation of the X-ray power-law, suggesting that the UV to X-ray spectrum of NGC 3998 is consistent with a power-law over 5 decades in energy. The SED of NGC 3998 is consistent with both RIAF models and a Comptonized thin-disk model (i.e., as expected to be found in Seyfert galaxies), both of which can account for the UV to X-ray spectrum of NGC 3998. None of the accretion models account for the compact radio emission in NGC 3998 which is probably dominated by a jet. The “pure” thin-disk model also does not account the mid-IR emission, although a truncated thin-disk surrounding an inner RIAF fits the mid-IR to X-ray spectrum well (with the near-IR to optical region dominated by extra-nuclear flux). If the accretion is dominated by an RIAF then the transition radius is $\gtrsim 300R_s$ and the \dot{m} is $\sim 3 \times 10^{-3}$ (at $\sim 300R_s$ in the models with $p > 0$). In either case the inner radius of the thin disk is probably $\gtrsim 100R_s$ in order to account for the lack of X-ray reflection features. If the accretion is dominated by a Comptonized thin disk that extends to a radius of $3R_s$, then the accretion rate in the disk is in the range $10^{-6} - 10^{-5}$ in Eddington units and the lack of Fe-K emission may be due to an ionized accretion disk. Finally, a jet model may be consistent with the radio and X-ray flux, and jet emission may also be responsible for the mid-IR and optical/UV flux.

This work was supported by NASA grants NAG5-11378 and NAG5-11572. Y. T. is supported by the Japan Society for the Promotion of Science. E. Q. received support by NASA ATP grant NAG5-12043 and a Sloan Foundation Fellowship. We made use of the High Energy Archive and Research Center at NASA/GSFC and the NASA Extragalactic Database. We thank the anonymous referee for useful comments that improved this paper.

REFERENCES

- Alonso-Herrero, A., Rieke, M., Rieke, G., & Shields, J. 2000, *ApJ*, 530, 688
 Awaki, H., Koyama, K., Kunieda, H., Takano, S., Tawara, Y., & Ohashi, T. 1991, *ApJ*, 366, 88
 Ball, G., Narayan, R. & Quataert, E. 2001, *ApJ*, 552, 221
 Ballantyne, D. & Ross, R. 2002, *MNRAS*, 332, 777
 Becker, R., White, R., & Edward, A. 1991, *ApJS*, 75, 1
 Blandford, R. & Begelman, M. 1999, *MNRAS*, 303, L1
 Bradt, H. & McClintock, J. 1983, 21, 13
 Burstein, D., Jones, C., Forman, W., Marston, A., & Marzke, R. 1997, *ApJS*, 111, 163
 Cardelli, J., Clayton, G., & Mathis, J. 1989, *ApJ*, 345, 245
 Condon, J. et al. 1998, *AJ*, 115, 1693
 Condon, J. & Dressel, L. 1978, *ApJ*, 221, 456
 David, L., Jones, C., & Forman, W. 1992, *ApJ*, 388, 82
 Di Matteo, T., Quataert, E., Allen, S., Narayan, R. & Fabian, A. 2000, *MNRAS*, 311, 507
 Done, C. & Nayakshin, S. 2001, *MNRAS*, 328, 616
 Elvis, M. et al. 1994, *ApJS*, 95, 1
 Fabbiano, G., Fassnacht, C., & Trinchieri G. 1994, *ApJ*, 434, 67
 Fabbiano, G. et al. 2003, 588, 175
 Filho, M., Barthel, P. & Ho, L. C. 2002, *A&A*, 385, 425
 Foschini, L., et al. 2002, *A&A*, 392, 817
 Frank, J., King, A., & Raine, D. 2002, *Accretion Power in Astrophysics*, Cambridge University Press, Cambridge
 Frogel, J., Persson, S., Aaronson, M. & Matthews, K. 1978, *ApJ*, 220, 75
 Hasinger, G. et al. 2001, *A&A*, 365, L45
 Hawley, J. F. & Balbus, S. A., 2002, *ApJ*, 573, 738
 Heckman, T. 1980, *A&A*, 87, 152
 Ho, L. C., Filippenko, A., & Sargent, W. 1997, *ApJS*, 112, 391
 Ho, L.C. 1999, *ApJ*, 516, 672
 Hornschemeier, A. et al. 2003, *ApJ*, 126, 575
 Hua, X.-M. & Titarchuk, L. 1995, *ApJ*, 449, 188
 Hummel, E. 1980, *A&AS*, 41, 151
 Hummel, E., Fanti, C., Parma, P., & Schilizzi, R. 1982, *A&A*, 114, 400
 Hummel, E., van der Hurst, J. M., & Dickey, J. M. 1984, *A&A*, 134, 207
 Igumenshchev, I. V., & Abramowicz, M. A. 1999, *MNRAS*, 303, 309
 Igumenshchev, I. V., & Abramowicz, M. A. 2000, *ApJS*, 130, 463
 Jenkins, E. & Savage, B. 1974, *ApJ*, 187, 243
 Knapp, G., van Driel, W., & van Woerden, H., 1985, *A&A*, 142, 1
 Longmore, A. & Sharples, R. 1982, *MNRAS*, 201, 111
 Mahadevan, R. 1997, *ApJ*, 477, 585
 Markoff, S., Falcke, H. & Fender, R. 2001, *A&A*, 372, L25
 Markoff, S., Nowak, M., Corbel, S., Fender, R., & Falcke, H. 2003, *A&A*, 397, 645
 McElroy, D. 1995, *ApJS*, 100, 105
 Monet, D. et al. 2003, *AJ*, 125, 984
 Mushotzky, R., Done, C., & Pounds, K. 1993, *ARA&A*, 31, 717
 Murphy, E., Lockman, F., Laor, A., & Elvis, M. 1996, *ApJS*, 105, 369
 Nandra, K., George, I., Mushotzky, R., Turner, T. & Yaqoob, T. 1997a, *ApJ*, 476, 70
 Nandra, K., George, I., Mushotzky, R., Turner, T. & Yaqoob, T. 1997b, *ApJ*, 477, 602
 Nandra, K., George, I., Mushotzky, R., Turner, T. & Yaqoob, T. 1997c, *ApJ*, 488, L91

- Narayan, R., Mahadevan, R. & Quataert, E. 1998,
Narayan, R. & Yi, I. 1994, ApJ, 428, L13
Norman, C. et al. 2004, ApJ, submitted
Pellegrini, S., Cappi, M., Bassani, L., Della Ceca, R., & Palumbo, G. 2000, *ã*, 360, 878
Pellegrini, S. et al. 2003, ApJ, 585, 677
Perna, R., Raymond, J. & Narayan, R. 2000, ApJ, 541, 898
Pietrini, P. & Krolik, J. 1995, ApJ, 447, 526
Proga, D. & Begelman, M. 2003, ApJ, 592, 767
Ptak, A., Yaqoob, T., Mushotzky, R., Serlemitsos, P., & Griffiths, R. 1998, ApJ, 501, L37
Ptak, A., Serlemitsos, P., Yaqoob, T., & Mushotzky, R. 1999, ApJS, 120, 179
Ptak, A. & Griffiths, R. 2002, ADASS 2002 proceedings, in press, astro-ph/0303104
Quataert, E. & Narayan, R. 1999, ApJ, 520, 298
Quataert, E., Di Matteo T., Narayan, R. & Ho, L. 1999, ApJ, 525, L89
Quataert, E. & Gruzinov, A., 2000, ApJ, 539, 809
Roberts, T. & Warwick, R. 2000, MNRAS, 315, 98
Reichert, G., Branduardi-Raymont, G., Filippenko, A., Mason, K., Puchnarewicz, E., & Wu, C.-C. 1992, 387, 536
Rees, M. J., Begelman, M. C., Blandford, R. D., & Phinney, E. S., 1982, Nature, 295, 17
Rengelink, R. et al. 1997, Astron. Astrophys. Suppl., 124, 25
Rybicki, G. & Lightman, A. 1979, Radiative Processes in Astrophysics (New York: John Wiley & Sons)
Snowden, S. 2002, from ESTEC Symposium 'New Visions of the X-ray Universe in the *XMM-Newton* and *Chandra* Era', astro-ph/0203311
Stone, J. M., Pringle, J. E., & Begelman, M. C. 1999, MNRAS, 310, 1002
Strickland, D. et al. 2001, ApJ, 560, 707
Szokoly, P. et al. 2004, ApJ, submitted, astro-ph/0312324
Terashima, Y., Iyomoto, N., Ho, L. C. & Ptak, A. 2002, ApJS, 139, 1
Titarchuk, L. 1994, ApJ, 434, 570
Tonry, J. et al. 2001, ApJ, 546, 681
Tremaine, S., et al. 2002, ApJ, 574, 740
White, R. & Becker, R. 1992, ApJS, 79, 331
Willner, S., Elvis, M., Fabbiano, G., Lawrence, A. & Ward, M. 1985, ApJ, 299, 443
Yaqoob, T. & Padmanabhan, U. 2002, from the proceedings of "Active Galactic Nuclei: from Central Engine to Host galaxy", eds. S. Collin, F. Combes, & I. Shlosman, in press (astro-ph/0211349)
Yuan, F., Markoff, S., Falcke, H., & Biermann, P. 2002, A&A, 391, 139

